This is a repository copy of *Microbial Blooms Triggered Pyrite Framboid Enrichment and Oxygen Depletion in Carbonate Platforms Immediately After the Latest Permian Extinction*.

White Rose Research Online URL for this paper:
https://eprints.whiterose.ac.uk/186479/

Version: Published Version

Article:

Chen, Z-Q, Fang, Y, Wignall, PB orcid.org/0000-0003-0074-9129 et al. (6 more authors) (2022) Microbial Blooms Triggered Pyrite Framboid Enrichment and Oxygen Depletion in Carbonate Platforms Immediately After the Latest Permian Extinction. Geophysical Research Letters, 49 (7). e2021GL096998. ISSN 0094-8276

https://doi.org/10.1029/2021GL096998

© 2022. American Geophysical Union. All Rights Reserved. This is the final version of the following article: Chen, Z.-Q., Fang, Y., Wignall, P. B., Guo, Z., Wu, S., Liu, Z., et al. (2022). Microbial blooms triggered pyrite framboid enrichment and oxygen depletion in carbonate platforms immediately after the latest Permian extinction. Geophysical Research Letters, 49, e2021GL096998, which has been published in final form at https://doi.org/10.1029/2021GL096998. An edited version of this paper was published by AGU. Copyright 2022 American Geophysical Union.

Reuse

Items deposited in White Rose Research Online are protected by copyright, with all rights reserved unless indicated otherwise. They may be downloaded and/or printed for private study, or other acts as permitted by national copyright laws. The publisher or other rights holders may allow further reproduction and re-use of the full text version. This is indicated by the licence information on the White Rose Research Online record for the item.

Takedown

If you consider content in White Rose Research Online to be in breach of UK law, please notify us by emailing eprints@whiterose.ac.uk including the URL of the record and the reason for the withdrawal request.

eprints@whiterose.ac.uk
https://eprints.whiterose.ac.uk/

Geophysical Research Letters

RESEARCH LETTER

10.1029/2021GL096998

Microbial Blooms Triggered Pyrite Framboid Enrichment and Oxygen Depletion in Carbonate Platforms Immediately After the Latest Permian Extinction

Zhong-Qiang Chen[1], Yuheng Fang[1], Paul B. Wignall[2], Zhen Guo[1], Siqi Wu[1], Ziliang Liu[1], Rongqin Wang[1], Yuangeng Huang[1], and Xueqian Feng[1]

[1]State Key Laboratory of Biogeology and Environmental Geology, China University of Geosciences, Wuhan, China, [2]School of Earth and Environment, University of Leeds, Leeds, UK

Key Points:

- A total of 17,306 pyrite framboids are analyzed in size and morphology from the Permian-Triassic boundary beds of 26 sections, South China
- Framboids were absent in ramp to basin and shallow, nonmicrobialite platforms after the extinction, but occurred in coeval microbialites
- Microbe bloom/microbialite growth was not triggered by reducing condition, but stimulated dysoxic water mass and triggered framboid growth

Supporting Information:

Supporting Information may be found in the online version of this article.

Correspondence to:

Z.-Q. Chen,
zhong.qiang.chen@cug.edu.cn

Citation:

Chen, Z.-Q., Fang, Y., Wignall, P. B., Guo, Z., Wu, S., Liu, Z., et al. (2022). Microbial blooms triggered pyrite framboid enrichment and oxygen depletion in carbonate platforms immediately after the latest Permian extinction. *Geophysical Research Letters*, *49*, e2021GL096998. https://doi.org/10.1029/2021GL096998

Received 12 NOV 2021
Accepted 20 MAR 2022

Abstract

Redox variations across the Permian-Triassic boundary (PTB) have long been debated, especially during the proliferation of PTB microbialites. Here, we report redox fluctuations across the PTB to evaluate links between the two based on pyrite framboid analysis from basin to platform settings in South China. During the end-Permian extinction, abundant framboids indicate a widespread anoxia that was likely a direct cause of extinction. In the earliest Triassic (*Hindeodus parvus* conodont zone), pyrite framboids were absent in ramp to basin and shallow, nonmicrobialite platform sections. In contrast, the coeval microbialites yield abundant framboids indicative of dysoxia. The fact that framboids were only confined to PTB microbialites and absent in other habitats indicates that microbe bloom may have stimulated dysoxic watermass and triggered the framboid growth within microbe aggregates. Thus, microbialites were not built in reducing settings, but instead, microbial proliferation caused local, dysoxia within shallow oxygenated platforms after the extinction.

Plain Language Summary

The widespread occurrence of microbialites immediately after the end-Permian extinction has attracted interest about their formation conditions. Microbialites are generally believed to be formed during microbial bloom in reducing conditions linked to the mass extinction. However, the cause-and-effect relationship between microbe bloom and reducing states of seawater has long been disputed. Our new results based on analyses of 17,306 pyrite framboid diameters and morphologies derived from various Permian-Triassic boundary sections in South China show that microbialite formation (microbial bloom) was not triggered by reducing waters upwelled from deeper water masses, instead, it caused local, dysoxic areas within oxygenated platforms after the end-Permian crisis.

1. Introduction

The nature of redox changes before, during, and after the latest Permian mass extinction (LPME) have long been debated (Cao et al., 2009; Clapham & Payne, 2011; Wignall & Hallam, 1993; Wignall & Twitchett, 2002; Zhang et al., 2018). The significance of microbialite development immediately after the LPME, and the associated oxygenation levels, is a further controversial aspect of the crisis (Baresel et al., 2017; Z. Q. Chen et al., 2019; Kershaw et al., 2012, 2018; Liao et al., 2017; G. M. Luo et al., 2014; Wignall et al., 2020). Did prevailing oxygen-poor conditions facilitate microbialite growth by suppressing grazing organisms? Pyrite framboids have been widely employed to evaluate paleo-redox states (Bond & Wignall, 2010; Y. G. Huang et al., 2019; Wacey et al., 2015; W. Wang et al., 2021). Here, we present analytical results of pyrite framboids across the Permian-Triassic boundary (PTB) from various sections in South China, including 3 nonmicrobialite platform sections, 11 microbialite-bearing platform sections, 1 ramp section, and 8 intraplatform basinal sections (Table S1 in Supporting Information S1; Figure 1b). The study aims to reconstruct redox histories before, during, and after the LPME in these diverse environmental settings, and to test the relationship between redox changes associated with mass extinction and microbial development.

During the P-Tr transition, the South China Block (SCB) was located in tropical latitudes of the eastern Paleo-Tethys Ocean (Figure 1a). A major carbonate platform called the Yangtze Platform developed in central part of the SCB, and was flanked by ramps on its northern and southern margins that extended into the Qinling sea and Nanpanjiang basin, respectively (Figure 1a). In this study, seven sections were sampled for pyrite analysis: Liangfengya (LFY), Zunyi (ZY), Yangou (YG), Tieshikou (TSK), Yudongzi (YDZ), Chaohu (CH), and Shangsi (SS). Among them, five sections are of shallow platform facies: LYF, ZY, YG, TSK, and YDZ (Figure 1a). The YG,

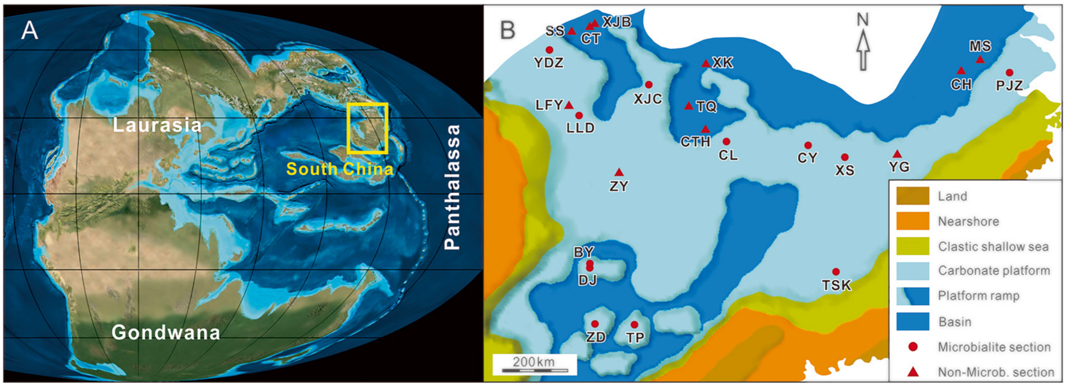

Figure 1. Paleogeographic map during the Permian-Triassic (P-Tr) transition. (a) Location of the South China Block (SCB) (Scotese & Schettino, 2017). (b) Paleogeographic settings of the 23 studied sections in the SCB (see Table S1 in Supporting Information S1). XJB, Xiaojiaba; CT, Changtan; SS, Shangsi; YDZ, Yudongzi; LFY, Liangfengya; LLD, Laolongdong; XJC, Xiajiacao; TQ, Tianqiao; XK, Xiakou; CTH, Changtanhe; CL, Cili; ZY, Zunyi; BY, Bianyang; DJ, Dajiang; ZD, Zuodeng; TP, Taiping; CY, Chongyang; XS, Xiushui; YG, Yangou; TSK, Tieshikou; CH, Chaohu; MS, Meishan; PJZ, Panjiazhuang.

LFY, and ZY sections record continuous carbonate deposition during the P-Tr transition, with shallow platform bioclastic or oolitic limestones of the uppermost Changxing Formation overlain by alternating marlstone and mudstone of the basal Triassic Daye/Feixianguan Formation. Of these, both LFY and ZY sections were located in relatively deep locations within the interior of the Yangtze Platform, while the YG section was located on the northern margin of the eastern wing of the Yangtze Platform. A hiatus is developed in many shallow-water PTB sites due to sea-level fall but continuous sedimentation of shallow water oolitic limestone occurred at YG probably due to rapid subsidence adjacent to the faulted platform margin at this location (Feng et al., 1997; H. Zhao et al., 2021; Zhu et al., 1994). At YDZ, the uppermost Permian bioclastic limestone is overlain unconformably by a basal Triassic microbialite unit. The TSK section consists of shallow platform bioclastic limestone in the upper Permian portion, transitioning to ramp facies (thin-bedded muddy limestone) in the uppermost Permian, and basinal mudstone in the lowest Triassic (Figure 2) which yields small bowl-like microbialites (Yang et al., 2019). The other two sections (CH and SS) are basinal and comprise uppermost Permian siliceous shale and cherty limestone overlain by the basal Triassic marlstone and mudstone of the basal Daye/or Feixianguan Formation. In addition, 16 additional and previously studied sections (including 8 microbialite-bearing sections) were also included in our regional redox mapping (Table S1 in Supporting Information S1). Results of former pyrite framboid analyses of the Meishan (MS) and Dajiang (DJ) sections have been re-examined due to slightly different analytical methods and standards used in various studies and are presented here (Z. Q. Chen et al., 2015; Y. G. Huang et al., 2017; Li et al., 2016).

Conodont zones across the PTB are well established in South China, and here they are divided into four phases. Phase 1 is equivalent to *Clarkina yini* zone (or upper *C. changxingensis* zone) and predates the LPME. Phase 2 corresponds to the *C. meishanensis*, *Hindeodus changxingensis*, and *C. taylorae* zones, the interval of mass extinction and its immediate aftermath. Phase 3 is equivalent to the *Hindeodus parvus* zone. The PTB is placed at the base of the *parvus* zone, and the majority of microbialites formed in this interval. In microbialite sections, Phase 2 is often absent due to a regional regression represented by an irregular contact at the base of the microbialite (Bagherpour et al., 2017; Foster et al., 2020; Kershaw et al., 2012; H. F. Yin et al., 2014). Phase 4 is defined by the conodonts *Hindeodus staeschei*, *Isarcica lobata*, and *I. isarcica* zones and equates the broadly defined *I. isarcica* zone in many earlier publications for these sections studied here.

Carbonate and organic carbon isotopes show a pronounced negative excursion around the LPME horizon, providing additional age constraint. Detailed descriptions as well as conodont biostratigraphic and carbon isotopic chemostratigraphic correlations of the studied sections (Figure S1 in Supporting Information S1) are provided in online supplementary data.

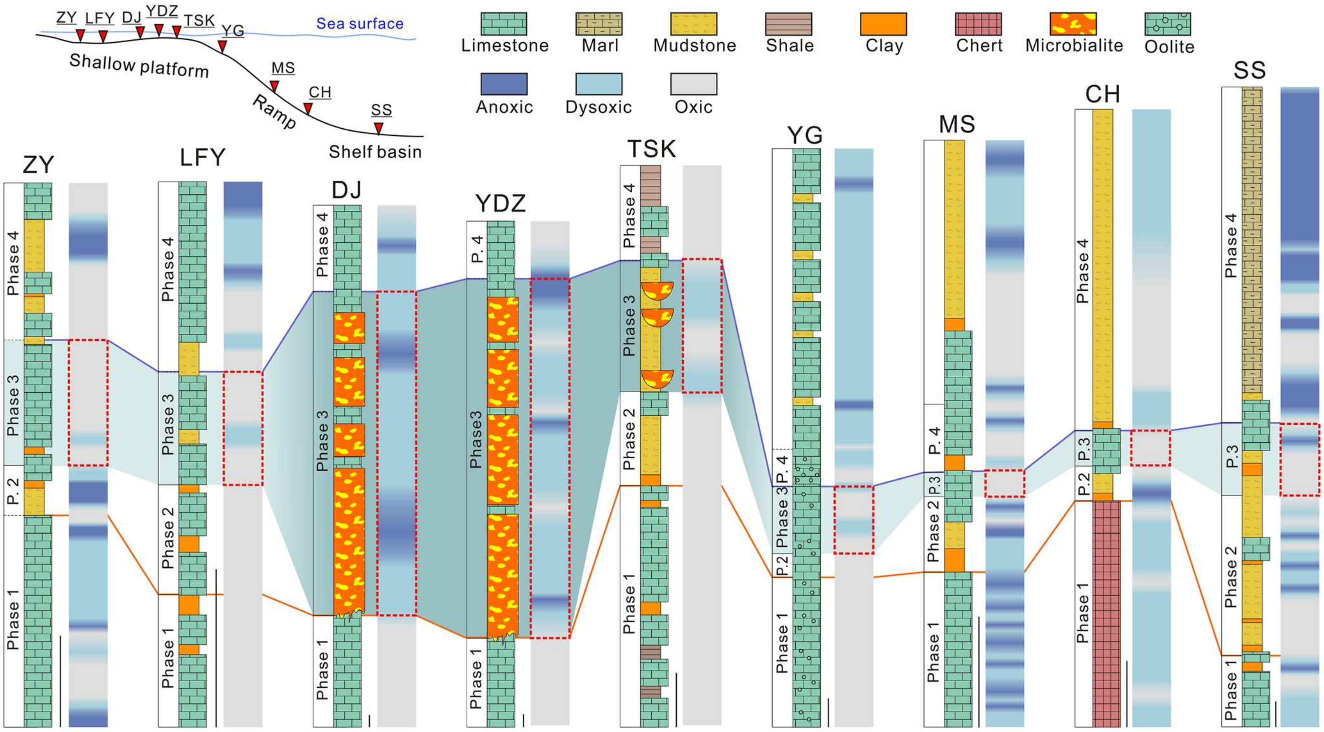

Figure 2. Correlations of P-Tr paleoredox condition changes among nine sections representing various water-depth settings in South China. Phase 3 is highlighted. Abbreviations are identical with Figure 1. Detailed conodont zones and framboid size distributions are shown in Figure S2 in Supporting Information S1. Scale bar = 0.5 m.

2. Materials and Methods

A total of 12,441 pyrite framboid grains were measured, and the data combined with published size measurements on 4,865 framboids from 23 P-Tr boundary sections across South China. The newly studied sections include: three nonmicrobialite platform sections (LFY, ZY, YG), two microbialite platform sections (YDZ, TSK), and three intraplatform basin facies sections (CH, SS) (Figure 1b). A total of 16 sections cited here include: 8 microbialite platform sections (Xiushui, Chongyang, Xiajiacao, Cili, Zuodeng, Laolongdong, Panjiazhuang, Taiping, and Dajiang; Table S1 in Supporting Information S1), 1 ramp section (MS), and 6 intraplatform basin sections (Changtanhe, Chaotian, Tianqiao, Bianyang, Xiaojiaba, and Xiakou; Table S1 in Supporting Information S1). These framboids were employed for size distribution and morphologic analyses.

Polished blocks (approximately 2 cm × 2 cm) of the samples were examined for framboid analysis using the Field Emission Scanning Electron Microscope Hitachi SU8010 at the State Key Laboratory of Biogeology and Environmental Geology, China University of Geosciences (Wuhan). Detailed experimental procedure and measurement bias controls follow Y. G. Huang et al. (2019). The standards for size distribution and morphology of framboids are modified from that of Bond and Wignall (2010), and are applied to distinguish four redox levels: euxinic, anoxic, dysoxic, and oxic conditions of water columns. Pyrite-size distributions are also evaluated using crossplots of mean framboid size (M) versus standard deviation (SD) (Wignall & Newton, 1998; Wilkin et al., 1996). On such a crossplot, the boundary separating euxinic from oxic-dysoxic facies was determined as: $M = -3.3 \times SD + 14$ (Wignall & Newton, 1998), where M is the mean diameter of framboids, and SD represents their standard deviation. Both framboid size and morphology criteria (Bond & Wignall, 2010) and the M-SD crossplot are utilized here to reconstruct marine redox states before, during and after the LPME.

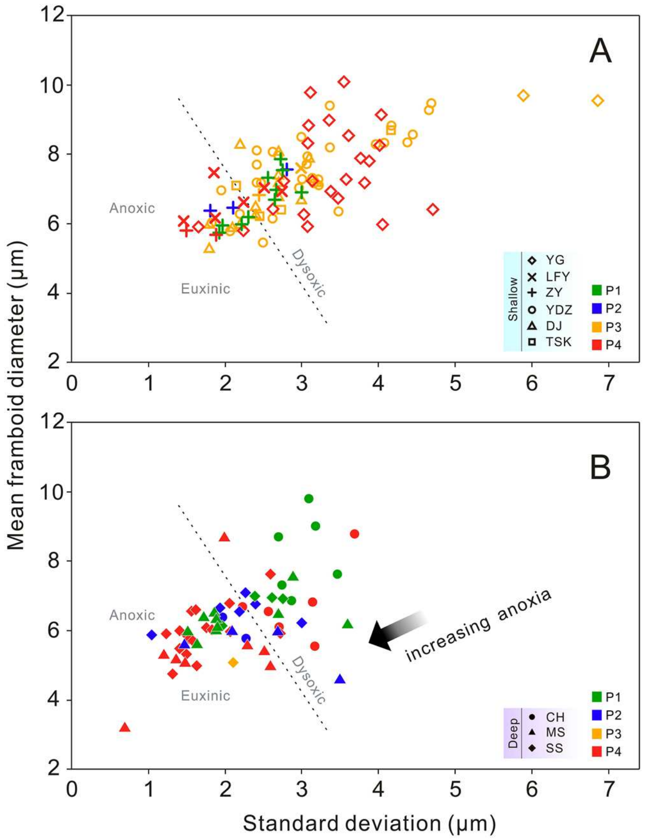

Figure 3. Mean - standard deviation plots of studied sections. (a) Plots of shallow platform sections. (b) Plots of deeper ramp and basinal sections. P1-P4 represent Phases 1–4. The dysoxic/anoxic-euxinic boundary is from Wilkin et al. (1996).

3. Results

3.1. Spatiotemporal Distributions of Pyrite Framboids and Redox Interpretation

In Phase 1, all microbialite sections and most nonmicrobialite sections on shallow platforms lack pyrite framboids (LYF to YG; Figure 2), except for ZY section that yields small framboids (4–8 μm in diameter) at several horizons, with a narrow size range and few crystals (Figure S2 in Supporting Information S1). Of the ZY samples, four and five samples had framboids that indicate anoxic and dysoxic conditions, respectively in mean-standard-deviation (M-SD) plots (Figure 3). In contrast, framboids were abundant in relatively deeper sections during Phase 1. Most samples from a ramp setting (MS) yield small framboids (approximately 6 μm in diameter), with a narrow size range and rare crystals, suggesting anoxia (Figure 3 and Figure S2 in Supporting Information S1). However, sections from basinal locations in Phase 1 lack framboids, although some horizons yield framboids of 6–10 μm diameter that fall into the dysoxic area in M-SD plots (Figure 3 and Figure S2 in Supporting Information S1).

Phase 2 framboids become abundant in the *C. meishanensis* and *H. changxingensis* zones in ramp facies before becoming rare in the *C. taylorae* zone (Figure S2 in Supporting Information S1). Most framboids are 4–6 μm in diameter, with a narrow size range, and fall into the anoxic area in the M-SD plot (Figure 3 and Figure S2 in Supporting Information S1). The rarity of pyrite crystals at this time is also typical of anoxic conditions (Bond & Wignall, 2010). The same interval in the deeper intraplatform basin sections (CH, SS) contains framboids in the *C. meishanensis* zone and alternations of framboid-rich and framboid-barren horizons in *H. changxingensis* and *C. taylorae* zones (Figure S2 in Supporting Information S1). The framboids from these two horizons are around 6 and 6–8 μm in mean diameter, respectively, and they fall into the anoxic and dysoxic areas, respectively in M-SD plots (Figure 3), indicating widespread oxygen-poor conditions during the LPME, ameliorating somewhat in its immediate aftermath in deeper water settings. All microbialite sections lack Phase 2 strata because of a hiatus at this level but most of the non-microbialite sections, from intraplatform basins (YG, LFY, TSK) do not yield any framboids. The ZY section, however, yields occasional framboids in the *C. taylorae* zone (Figure S2 in Supporting Information S1). Thus, oxic conditions prevailed at this time in the local depocentres that persisted on the platform.

During Phase 3, the basinal sections (CH, SS) surprisingly do not yield any framboids, suggesting oxic conditions (Figure 2 and Figure S2 in Supporting Information S1). A few large framboids and pyrite crystals occurred in the same interval in a ramp setting (MS), again indicating good oxygenation (Z. Q. Chen et al., 2015; Y. G. Huang et al., 2017). Framboid occurrences are markedly different in shallow platform sections in this phase. Abundant framboids of 6–10 μm in diameter occur in all microbialite sections (DJ, YDZ, and others), pointing to dysoxic conditions. In contrast, no framboids are found in this interval in non-microbialite platform locations (ZY, LFY, YG; Figure 2 and Figure S2 in Supporting Information S1), reflecting oxic redox states. The TSK section yields some framboids, but they are found in the bowl-like microbialites, whilst the surrounding mudstone lacks framboids.

In Phase 4, framboids have very different stratigraphic distributions among various sections. The deeper ramp and basinal sections (MS, SS) yield abundant tiny framboids that fall into the anoxic and euxinic areas in M-SD plots (Figure 3), while the CH and TSK sections of the same facies contain rare or lack framboids. The shallow platform nonmicrobialite sections (ZY, YG, LFY) yield framboids indicative of dysoxic to anoxic conditions. The microbialite DJ section yields framboids suggestive of anoxic conditions, but another microbialite section (YDZ) lacks framboids, indicative of oxic conditions (Figure 2 and Figure S1 in Supporting Information S1).

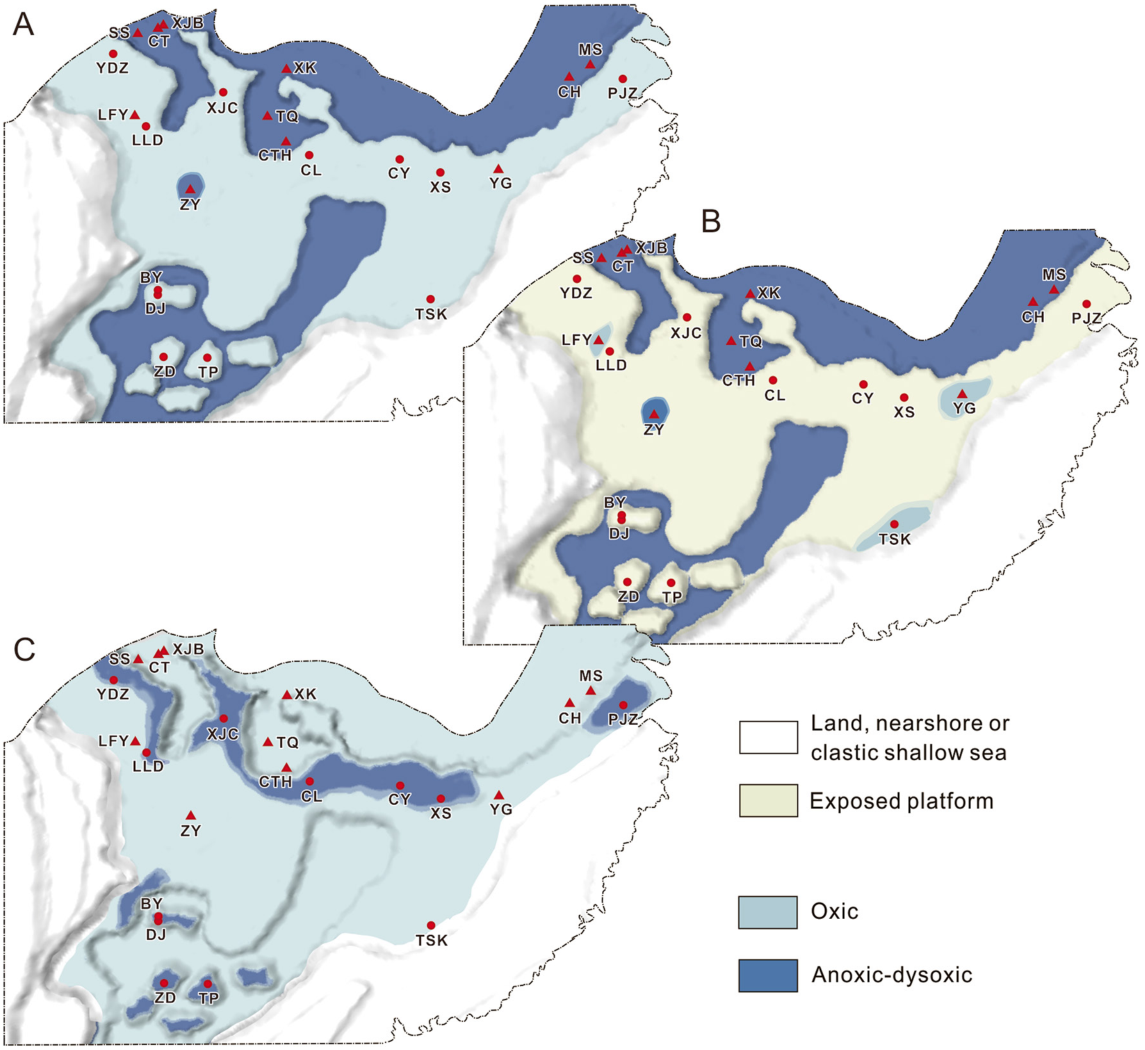

Figure 4. Redox mapping over the P-Tr transition (from Phase 1 to Phase 3) in South China. (a)–(c) Redox maps showing spatiotemporal distributions of reducing water masses during Phases 1–3.

3.2. Spatial Redox Variations Over the P-Tr Transition

Framboid analysis shows that most habitats in shallow platforms in South China were oxygenated prior to the LPME (Phase 1), except for few localities (i.e., ZY) where dysoxia developed (Figure 4). Anoxic water columns prevailed in ramp settings (MS), with episodic incursion of dysoxic to oxic water masses (Figure 4a). During the LPME (Phase 2), anoxia was extensive, indicating a close link between anoxia and the biotic crisis, as also indicated by geochemical proxies (i.e., U isotopes; Elrick et al., 2017; Zhang et al., 2018). Some of the deep locations in the interior of the Yangtze Platform (i.e., ZY) also developed anoxic waters, while all platform locations that would later go on to develop microbialites were subaerially exposed at this time (H. F. Yin et al., 2014).

Remarkably, the development of anoxia in Phase 3 was the opposite to that seen in Phase 2 in South China (Figure 4c). Dysoxia was confined to the microbialite sites in shallow platforms, whilst oxygenated water columns prevailed in shallow nonmicrobialite platform locations, ramp, and deeper basin settings (Figure 4c). Pyrite framboids at this time are embedded within microbialites, but are absent from the surrounding basinal mudstone (see TSK section). This indicates that microbial growth stimulated the development of dysoxia in interstitial waters. Oxygen-depleted watermasses expanded once again in Phase 4 and spread into shallow and deeper settings (Figure 4d).

4. Discussion

4.1. Redox Variations Over the P-Tr Transition in South China

In South China, framboid data show that episodic anoxic and dysoxic water masses prevailed in ramp and deeper intraplatform basin settings prior to mass extinction, whilst adjacent platforms were mostly oxic, except for few localities (i.e., ZY) that were occasionally invaded by oxygen-poor water masses (Figure 2). This intermittent dysoxia is also revealed in ramp and restricted platform settings by biomarker and sulfur isotopic analyses (Cao et al., 2009; Grice et al., 2005; Y. A. Shen et al., 2011). Deeper basinal sections have few framboid-bearing horizons and lack small populations of framboid diameter indicating only occasional oxygen restriction in these settings (Figure 4). Thus, in Phase 1 the most oxygen-restricted conditions developed in ramp locations perhaps due to the presence of a mid-depth oxygen-minimum zone (OMZ; Figure 4a). Alternatively, a depletion of Fe^{2+} in water column may also cause the rarity of framboids in deeper basinal settings because intensive anoxia in mid-depth waters have already removed Fe^{2+} as pyrites. However, this is not the case for the P-Tr records because marine anoxia spread over all water-depth settings during Phase 2 (LPME), but pyrite framboids were abundant in deep basinal sections, implying that the water columns were not short of Fe^{2+} at that time.

During Phase 2, temporal distribution of framboids indicates widespread anoxia coincident with the LPME especially in deeper ramp and basin environments in South China, confirming the results from numerous other studies (Z. Q. Chen et al., 2015; Huang et al., 2017, 2019; Lau et al., 2016; Li et al., 2016; Payne et al., 2010; Wignall et al., 2016; Zhang et al., 2018). Most shallow platform sections (except for ZY) lack framboids in this horizon, although there is a widespread hiatus at this level in such settings (H. F. Yin et al., 2014). Overall, it appears the OMZ of Phase 1 expanded greatly into both deeper waters and sporadically spread to shallow water habitats during this stage.

During Phase 3, there was a major reoxidation of water masses in almost all settings (from deep basin to shallow platform) except in microbialite sites which were dysoxic (Figure 4c). Even in ramp settings dysoxic to oxic conditions prevailed, implying only weak OMZ development. In contrast, moderate-sized framboids are abundant in all microbialites (up to 11 sites across South China; Table S1 in Supporting Information S1), pointing to a dysoxic state (see below). This means that redox conditions switched rapidly from the widespread anoxia linking with the LPME (Phase 2) to an oxygenated state (Phase 3) soon after.

During Phase 4, redox conditions decline once again with euxinia/anoxia in ramp settings, and anoxia/dysoxia in intraplatform basins and (episodically) in shallow platforms (Figure 2). Clearly, Phase 4 witnessed the most widespread oxygen-poor watermasses among these four phases of the P-Tr transition and coincides with the aftermath of the second phase of mass extinction that eliminated many surviving taxa (Song et al., 2013). Sedimentary successions capping the PTB microbialites across South China are comprised of the mud-dominated calcareous strata, pointing to the rise in sea-level during Phase 4 (Z. Q. Chen et al., 2019; Kershaw et al., 2012; Yang et al., 2011). A coeval transgression was also indicated in other non-microbialite sections in South China (H. F. Yin et al., 2012, 2014). Accordingly, both the regional transgression and elevated reducing water masses may have resulted in the demise of microbialites across South China during Phase 4.

4.2. Enrichment of Pyrite Framboids and Oxygenation State of the Microbialites

Oxygenation state of the PTB microbialites has long been disputed due to conflicting evidence from different redox proxies (Bagherpour et al., 2017; Baresel et al., 2017; L. Chen et al., 2011; Collin et al., 2015; Ezaki et al., 2008; Heindel et al., 2018; Kershaw et al., 2018; Lau et al., 2016; Liao et al., 2017; G. M. Luo et al., 2013). The presence of framboids in all the PTB microbialite samples of Phase 3, but their absence from other platform facies indicates that environments were generally oxic but that microbial carbonate habitats were conducive to pyrite framboid growth. Previous suggestions that deeper anoxic waters upwelled or overturned and spilled into areas of microbialite growth (Baresel et al., 2017; Liao et al., 2017; G. M. Luo et al., 2013) are shown to be invalid by our results because ramp and intraplatform basin settings were mostly oxic at that time (Figure 4c). This inference is also strengthened by the presence of abundant framboids, indicative of a dysoxic state, in stromatolite nodules embedded within mudstone of intraplatform basin facies, and their absence in the surrounding mudstone in TSK section (Yang et al., 2019). The microbial growth clearly created localized anoxic conditions favorable for the growth of framboids after the LPME. Thus, the shallow platforms were generally oxygenated except for local microbe-rich water masses, in which the flourishing of microbes resulted in local oxygen-poor habitats that stimulated the production of abundant moderate-sized framboids.

The post-extinction microbial bloom was interpreted as the elimination of metazoans that usually consume microbes in marine ecosystems after the LPME (Xie et al., 2005). Alternatively, global nitrogen isotopes ($\delta^{15}N$) showed strong denitrification across the LPME (Phase 2), followed by an enhanced nitrogen fixation in the earliest Triassic (Phase 3; Cao et al., 2009; C. Jia et al., 2012; G. M. Luo et al., 2011; Xie et al., 2010). Thus, the postextinction development of extensive microbialites was probably facilitated by diazotrophs (NH^{+4} self-sufficient by N-fixation) or fertilized by ambient NH^{+4} (Sun et al., 2019). Cyanobacterial proliferation in microbialites (G. M. Luo et al., 2013) was largely because many cyanobacteria have the ability of nitrogen fixation, and therefore were self-sufficient in a nitrate-depleted ocean. They may also have produced oxygen and nutrients for metazoans to grow within the microbialite ecosystem. This is why abundant and diverse metazoans inhibited microbialite ecosystems (Forel et al., 2013; Foster et al., 2019, 2020; Lehrmann et al., 2015; Yang et al., 2011), although their oxygenation state overall was dysoxic. This is why the PTB microbialites usually have little organic carbon burial, low contents of total organic carbon, and low productivities in South China (Algeo et al., 2013).

5. Conclusions

Analysis of 17,306 pyrite framboid diameters from 23 P-Tr boundary sections in South China, representing intraplatform basin, deep ramp, and shallow platform facies was undertaken in order to evaluate oxygenation variations across the PTB. The results show that redox variations were controlled by the expansion/contraction of oxygen minimum zones existing at moderate-depths in ramp habitats prior to the LPME. Anoxic water masses expanded considerably into deep basin and shallower ramp settings and episodically invaded shallow platforms at the time of mass extinction. The immediate aftermath of this crisis saw a major improvement of oxygenation levels across a broad range of environments, and the growth of microbialites that created localized anoxic conditions favorable for framboid formation. This interval did not witness upwelling of anoxic water masses as widely claimed. The shutdown of the microbialite ecosystems saw the rise in sea-level and the resumption of widespread anoxic conditions in the earliest Triassic.

Data Availability Statement

All supplementary data related to this paper is available at: https://doi.org/10.5281/zenodo.6383974.

Acknowledgments
This study is supported by three NSFC grants (41821001, 41830323, and 41930322) and by 111 Project of China (Grant No. BP0820004). It is a contribution to International Geosciences Program (IGCP) 630: "Permian and Triassic Integrated Stratigraphy and Climatic, Environmental and Biotic Extremes."

References

Algeo, T. J., Henderson, C. M., Tong, J., Feng, Q., Yin, H., & Tyson, R. V. (2013). Plankton and productivity during the Permian-Triassic boundary crisis: An analysis of organic fluxes. *Global and Planetary Change*, *105*, 52–67. https://doi.org/10.1016/j.gloplacha.2012.02.008

Bagherpour, B., Bucher, H., Baud, A., Brosse, M., Vennemann, T., Martini, R., & Guodun, K. (2017). Onset, development, and cessation of basal early Triassic microbialites (BETM) in the Nanpanjiang pull-apart basin, South China block. *Gondwana Research*, *44*, 178–204. https://doi.org/10.1016/j.gr.2016.11.013

Baresel, B., Bucher, H., Bagherpour, B., Brosse, M., Guodun, K., & Schaltegger, U. (2017). Timing of global regression and microbial bloom linked with the Permian-Triassic boundary mass extinction: Implications for driving mechanisms. *Scientific Reports*, *7*, 43630. https://doi.org/10.1038/srep43630

Bond, D. P. G., & Wignall, P. B. (2010). Pyrite framboid study of marine Permian-Triassic boundary sections: A complex anoxic event and its relationship to contemporaneous mass extinction. *Geological Society of America Bulletin*, *122*(7–8), 1265–1279. https://doi.org/10.1130/b30042.1

Cao, C. Q., Love, G. D., Hays, L. E., Wang, W., Shen, S. Z., & Summons, R. E. (2009). Biogeochemical evidence for euxinic oceans and ecological disturbance presaging the end-Permian mass extinction event. *Earth and Planetary Science Letters*, *281*(3–4), 188–201. https://doi.org/10.1016/j.epsl.2009.02.012

Chen, L., Wang, Y. B., Xie, S. C., Kershaw, S., Dong, M., Yang, H., et al. (2011). Molecular records of microbialites following the end-Permian mass extinction in Chongyang, Hubei Province, South China. *Palaeogeography, Palaeoclimatology, Palaeoecology*, *308*(1–2), 151–159. https://doi.org/10.1016/j.palaeo.2010.09.010

Chen, Z. Q., Tu, C. Y., Pei, Y., Ogg, J., Fang, Y. H., Wu, S. Q., et al. (2019). Biosedimentological features of major microbe-metazoan transitions (MMTs) from Precambrian to Cenozoic. *Earth-Science Reviews*, *189*, 21–50. https://doi.org/10.1016/j.earscirev.2019.01.015

Chen, Z. Q., Yang, H., Luo, M., Benton, M. J., Kaiho, K., Zhao, L. S., et al. (2015). Complete biotic and sedimentary records of the Permian-Triassic transition from Meishan section, South China: Ecologically assessing mass extinction and its aftermath. *Earth-Science Reviews*, *149*, 67–107. https://doi.org/10.1016/j.earscirev.2014.10.005

Clapham, M. E., & Payne, J. L. (2011). Acidification, anoxia, and extinction: A multiple logistic regression analysis of extinction selectivity during the middle and late Permian. *Geology*, *39*, 1059–1062. https://doi.org/10.1130/g32230.1

Collin, P. Y., Kershaw, S., Tribovillard, N., Forel, M. B., & Crasquin, S. (2015). Geochemistry of post-extinction microbialites as a powerful tool to assess the oxygenation of shallow marine water in the immediate aftermath of the end-Permian mass extinction. *International Journal of Earth Sciences*, *104*(4), 1025–1037. https://doi.org/10.1007/s00531-014-1125-3

Elrick, M., Polyak, V., Algeo, T. J., Romaniello, S., Asmerom, Y., Herrmann, A. D., et al. (2017). Global-ocean redox variation during the middle-late Permian through Early Triassic based on uranium isotope and Th/U trends of marine carbonates. *Geology*, *45*(2), 163–166. https://doi.org/10.1130/g38585.1

Ezaki, Y., Liu, J. B., Nagano, T., & Adachi, N. (2008). Geobiological aspects of the earliest Triassic microbialites along the southern periphery of the tropical Yangtze Platform: Initiation and cessation of a microbial regime. *PALAIOS*, *23*(5–6), 356–369. https://doi.org/10.2110/palo.2007.p07-035r

Feng, Z., Bao, Z., Wu, S., Li, Y., & Wang, G. (1997). *Lithofacies Palaeogeography of the Early and Middle Triassic of South China*. Petroleum Industry Press.

Forel, M. B., Crasquin, S., Kershaw, S., & Collin, P. Y. (2013). In the aftermath of the end-Permian extinction: The microbialite refuge? *Terra Nova*, *25*(2), 137–143. https://doi.org/10.1111/ter.12017

Foster, W. J., Heindel, K., Richoz, S., Gliwa, J., Lehrmann, D. J., Baud, A., et al. (2020). Suppressed competitive exclusion enabled the proliferation of Permian/Triassic boundary microbialites. *The Depositional Record*, *6*, 62–74. https://doi.org/10.1002/dep2.97

Foster, W. J., Lehrmann, D. J., Hirtz, J. A., White, M., Yu, M. Y., Li, J., & Martindale, R. C. (2019). Early Triassic benthic invertebrates from the Great Bank of Guizhou, South China: Systematic palaeontology and palaeobiology. *Papers in Palaeontology*, *5*(4), 613–656. https://doi.org/10.1002/spp2.1252

Grice, K., Cao, C. Q., Love, G. D., Bottcher, M. E., Twitchett, R. J., Grosjean, E., et al. (2005). Photic zone euxinia during the Permian-Triassic superanoxic event. *Science*, *307*(5710), 706–709. https://doi.org/10.1126/science.1104323

Heindel, K., Foster, W. J., Richoz, S., Birgel, D., Roden, V. J., Baud, A., et al. (2018). The formation of microbial-metazoan bioherms and biostromes following the latest Permian mass extinction. *Gondwana Research*, *61*, 187–202. https://doi.org/10.1016/j.gr.2018.05.007

Huang, Y. G., Chen, Z. Q., Algeo, T. J., Zhao, L. S., Baud, A., Bhat, G. M., et al. (2019). Two-stage marine anoxia and biotic response during the Permian-Triassic transition in Kashmir, northern India: Pyrite framboid evidence. *Global and Planetary Change*, *172*, 124–139. https://doi.org/10.1016/j.gloplacha.2018.10.002

Huang, Y. G., Chen, Z. Q., Wignall, P. B., & Zhao, L. S. (2017). Latest Permian to Middle Triassic redox condition variations in ramp settings, South China: Pyrite framboid evidence. *Geological Society of America Bulletin*, *129*(1–2), 229–243. https://doi.org/10.1130/b31458.1

Jia, C., Huang, J., Kershaw, S., Luo, G., Farabegoli, E., Perri, M. C., et al. (2012). Microbial response to limited nutrients in shallow water immediately after the end-Permian mass extinction. *Geobiology*, *10*(1), 60–71. https://doi.org/10.1111/j.1472-4669.2011.00310.x

Kershaw, S., Crasquin, S., Li, Y., Collin, P. Y., Forel, M. B., Mu, X., et al. (2012). Microbialites and global environmental change across the Permian-Triassic boundary: A synthesis. *Geobiology*, *10*(1), 25–47. https://doi.org/10.1111/j.1472-4669.2011.00302.x

Kershaw, S., Tang, H., Li, Y., & Guo, L. (2018). Oxygenation in carbonate microbialites and associated facies after the end-Permian mass extinction: Problems and potential solutions. *Journal of Palaeogeography-English*, *7*(1), 32–47. https://doi.org/10.1016/j.jop.2017.10.001

Lau, K. V., Maher, K., Altiner, D., Kelley, B. M., Kump, L. R., Lehrmann, D. J., et al. (2016). Marine anoxia and delayed Earth system recovery after the end-Permian extinction. *Proceedings of the National Academy of Sciences of the United States of America*, *113*(9), 2360–2365. https://doi.org/10.1073/pnas.1515080113

Lehrmann, D. J., Bentz, J. M., Wood, T., Goers, A., Dhillon, R., Akin, S., et al. (2015). Environmental controls on the genesis of marine microbialites and dissolution surface associated with the end-Permian mass extinction: New sections and observations from the Nanpanjiang basin, South China. *PALAIOS*, *30*(7), 529–552. https://doi.org/10.2110/palo.2014.088

Li, G. S., Wang, Y. B., Shi, G. R., Liao, W., & Yu, L. X. (2016). Fluctuations of redox conditions across the Permian-Triassic boundary: New evidence from the GSSP section in Meishan of South China. *Palaeogeography, Palaeoclimatology, Palaeoecology*, *448*, 48–58. https://doi.org/10.1016/j.palaeo.2015.09.050

Liao, W., Bond, D. P. G., Wang, Y. B., He, L., Yang, H., Weng, Z. T., & Li, G. S. (2017). An extensive anoxic event in the Triassic of the South China block: A pyrite framboid study from Dajiang and its implications for the cause(s) of oxygen depletion. *Palaeogeography, Palaeoclimatology, Palaeoecology*, *486*, 86–95. https://doi.org/10.1016/j.palaeo.2016.11.012

Luo, G. M., Wang, Y., Algeo, T. J., Kump, L. R., Bai, X., Yang, H., et al. (2011). Enhanced nitrogen fixation in the immediate aftermath of the latest Permian marine mass extinction. *Geology*, *39*, 647–650. https://doi.org/10.1130/g32024.1

Luo, G. M., Wang, Y. B. A., Grice, K., Kershaw, S., Algeo, T. J., Ruan, X. Y., et al. (2013). Microbial-algal community changes during the latest Permian ecological crisis: Evidence from lipid biomarkers at Cili, South China. *Global and Planetary Change*, *105*, 36–51. https://doi.org/10.1016/j.gloplacha.2012.11.015

Luo, G. M., Xie, S. C., Liu, D., & Algeo, T. J. (2014). Microbial influences on paleoenvironmental changes during the Permian-Triassic boundary crisis. *Science China Earth Sciences*, *57*(5), 965–975. https://doi.org/10.1007/s11430-014-4822-7

Payne, J. L., Turchyn, A. V., Paytan, A., DePaolo, D. J., Lehrmann, D. J., Yu, M. Y., & Wei, J. Y. (2010). Calcium isotope constraints on the end-Permian mass extinction. *Proceedings of the National Academy of Sciences of the United States of America*, *107*(19), 8543–8548. https://doi.org/10.1073/pnas.0914065107

Scotese, C. R., & Schettino, A. (2017). Chapter 3—Late Permian–early Jurassic paleogeography of Western Tethys and the world. In J. E. Soto, J. Flinch, & G. Tari (Eds.), *Permo-Triassic Salt Provinces of Europe, North Africa, and the central Atlantic: Tectonics and Hydrocarbon Potential* (pp. 57–95). https://doi.org/10.1016/b978-0-12-809417-4.00004-5

Shen, Y. A., Farquhar, J., Zhang, H., Masterson, A., Zhang, T. G., & Wing, B. A. (2011). Multiple S-isotopic evidence for episodic shoaling of anoxic water during Late Permian mass extinction. *Nature Communications*, *2*, 210. https://doi.org/10.1038/ncomms1217

Song, H. J., Wignall, P. B., Tong, J. N., & Yin, H. F. (2013). Two pulses of extinction during the Permian-Triassic crisis. *Nature Geoscience*, *6*(1), 52–56. https://doi.org/10.1038/ngeo1649

Sun, Y. D., Zulla, M. J., Joachimski, M. M., Bond, D. P. G., Wignall, P. B., Zhang, Z. T., & Zhang, M. H. (2019). Ammonium ocean following the end-Permian mass extinction. *Earth and Planetary Science Letters*, *518*, 211–222. https://doi.org/10.1016/j.epsl.2019.04.036

Wacey, D., Kilburn, M. R., Saunders, M., Cliff, J. B., Kong, C., Liu, A. G., et al. (2015). Uncovering framboidal pyrite biogenicity using nano-scale CNorg mapping. *Geology*, *43*(1), 27–30. https://doi.org/10.1130/g36048.1

Wang, W., Hu, Y. L., Muscente, A. D., Cui, H., Guan, C. G., Hao, J. L., & Zhou, C. M. (2021). Revisiting Ediacaran sulfur isotope chemostratigraphy with in situ nanoSIMS analysis of sedimentary pyrite. *Geology*, *49*(6), 611–616. https://doi.org/10.1130/g48262.1

Wignall, P. B., Bond, D. P. G., Sun, Y. D., Grasby, S. E., Beauchamp, B., Joachimski, M. M., & Blomeier, D. P. G. (2016). Ultra-shallow-marine anoxia in an Early Triassic shallow-marine clastic ramp (Spitsbergen) and the suppression of benthic radiation. *Geological Magazine*, *153*(2), 316–331. https://doi.org/10.1017/s0016756815000588

Wignall, P. B., Chu, D. L., Hilton, J. M., Dal Corso, J., Wu, Y. Y., Wang, Y., et al. (2020). Death in the shallows: The record of Permo-Triassic mass extinction in paralic settings, southwest China. *Global and Planetary Change*, *189*, 103176. https://doi.org/10.1016/j.gloplacha.2020.103176

Wignall, P. B., & Hallam, A. (1993). Griesbachian (earliest Triassic) palaeoenvironmental changes in the Salt Range, Pakistan and southeast China and their bearing on the Permo-Triassic mass extinction. *Palaeogeography, Palaeoclimatology, Palaeoecology*, *102*, 215–237. https://doi.org/10.1016/0031-0182(93)90068-t

Wignall, P. B., & Newton, R. (1998). Pyrite framboid diameter as a measure of oxygen deficiency in ancient mudrocks. *American Journal of Science*, *298*(7), 537–552. https://doi.org/10.2475/ajs.298.7.537

Wignall, P. B., & Twitchett, R. J. (2002). Extent, duration, and nature of the Permian-Triassic superanoxic event. In C. Koeberl, & K. G. MacLeod (Eds.), (Vol. 356, pp. 395–413). https://doi.org/10.1130/0-8137-2356-6.395.*Catastrophic Events and Mass Extinctions: Impacts and Beyond*

Wilkin, R. T., Barnes, H. L., & Brantley, S. L. (1996). The size distribution of framboidal pyrite in modern sediments: An indicator of redox conditions. *Geochimica et Cosmochimica Acta*, *60*(20), 3897–3912. https://doi.org/10.1016/0016-7037(96)00209-8

Xie, S., Pancost, R. D., Wang, Y., Yang, H., Wignall, P. B., Luo, G., et al. (2010). Cyanobacterial blooms tied to volcanism during the 5my Permo-Triassic biotic crisis. *Geology*, *38*, 447–450. https://doi.org/10.1130/G30769.1

Xie, S., Pancost, R. D., Yin, H., Wang, H., & Evershed, R. P. (2005). Two episodes of microbial change coupled with Permo/Triassic faunal mass extinction. *Nature*, *434*, 494–497. https://doi.org/10.1038/nature03396

Yang, H., Chen, Z. Q., Kershaw, S., Liao, W., Lu, E. L., & Huang, Y. G. (2019). Small microbialites from the basal Triassic mudstone (Tieshikou, Jiangxi, South China): Geobiologic features, biogenicity, and paleoenvironmental implications. *Palaeogeography Palaeoclimatology Palaeoecology*, *519*, 221–235. https://doi.org/10.1016/j.palaeo.2018.06.030

Yang, H., Chen, Z. Q., Wang, Y. B., Tong, J. A., Song, H. J., & Chen, J. (2011). Composition and structure of microbialite ecosystems following the end-Permian mass extinction in South China. *Palaeogeography, Palaeoclimatology, Palaeoecology*, *308*(1–2), 111–128. https://doi.org/10.1016/j.palaeo.2010.05.029

Yin, H. F., Jiang, H. S., Xia, W. C., Feng, Q. L., Zhang, N., & Shen, J. (2014). The end-Permian regression in South China and its implication on mass extinction. *Earth-Science Reviews*, *137*, 19–33. https://doi.org/10.1016/j.earscirev.2013.06.003

Yin, H. F., Xie, S., Luo, G., Algeo, T. J., & Zhang, K. (2012). Two episodes of environmental change at the Permian-Triassic boundary of the GSSP section Meishan. *Earth-Science Reviews*, *115*, 163–172. https://doi.org/10.1016/j.earscirev.2012.08.006

Zhang, F. F., Algeo, T. J., Romaniello, S. J., Cui, Y., Zhao, L. S., Chen, Z. Q., & Anbar, A. D. (2018). Congruent Permian-Triassic δ238U records at Panthalassic and Tethyan sites: Confirmation of global-oceanic anoxia and validation of the U-isotope paleoredox proxy. *Geology*, *46*(4), 327–330. https://doi.org/10.1130/G39695.1

Zhao, H., Lyu, Z. Y., Chen, Z. Q., Algeo, T. J., Orchard, M. J., Liu, Y. S., et al. (2021). Integrated biochemostratigraphy of the Permian-Triassic boundary beds in a shallow carbonate platform setting (Yangou, South China). *Global and Planetary Change*, *206*, 103583. https://doi.org/10.1016/j.gloplacha.2021.103583

Zhu, X. S., Wang, C. Y., Lü, Y., Mu, X. N., Zhang, L. X., Qin, Z. S., et al. (1994). Permian-triassic boundaries in Jiangxi, China. *Acta Micropalaeontologica Sinica*, *11*, 439–452.

References From the Supporting Information

Cao, C. Q., Wang, W., & Jin, Y. G. (2002). Carbon isotope excursions across the Permian-Triassic boundary in the Meishan section, Zhejiang Province, China. *Chinese Science Bulletin*, *47*(13), 1125–1129. https://doi.org/10.1360/02tb9252

Collin, P. Y., Kershaw, S., Soleau, S. C., & Feng, Q. (2009). Facies changes and diagenetic processes across the Permian–Triassic boundary event horizon, Great Bank of Guizhou, South China: A controversy of erosion and dissolution. *Sedimentology*, *56*, 677–693.

Fang, Y. H., Chen, Z. Q., Kershaw, S., Yang, H., & Luo, M. (2017). Permian-triassic boundary microbialites at Zuodeng section, Guangxi Province, South China: Geobiology and palaeoceanographic implications. *Global and Planetary Change*, *152*, 115–128. https://doi.org/10.1016/j.gloplacha.2017.02.011

Feng, Z., Bao, Z., Wu, S., Li, Y., & Wang, G. (1997). *Lithofacies palaeogeography of the early and middle Triassic of South China*. Petroleum Industry Press.

Foster, W. J., Lehrmann, D. J., Hirtz, J. A., White, M., Yu, M. Y., Li, J., & Martindale, R. C. (2019). Early Triassic benthic invertebrates from the Great Bank of Guizhou, South China: Systematic palaeontology and palaeobiology. *Papers in Palaeontology*, *5*(4), 613–656. https://doi.org/10.1002/spp2.1252

Gao, Q. L., Chen, Z. Q., Zhang, N., Griffin, W. L., Xia, W. C., Wang, G. Q., et al. (2015). Ages, trace elements and Hf-isotopic compositions of zircons from claystones around the Permian-Triassic boundary in the Zunyi Section, South China: Implications for nature and tectonic setting of the volcanism. *Journal of Earth Science*, *26*, 872–882.

Gorjan, P., Kaiho, K., Kakegawa, T., Niitsuma, S., Chen, Z. Q., Kajiwara, & Nicora, A. (2007). Paleoredox, biotic and sulfur-isotopic changes associated with the end-Permian mass extinction in the Western Tethys. *Chemical Geology*, *244*, 483–492. https://doi.org/10.1016/j.chemgeo.2007.07.003

He, L., Wang, Y. B. A., Woods, A., Li, G. S., Yang, H., & Liao, W. (2013). An oxygenation event occurred in deep shelf settings immediately after the end-Permian mass extinction in South China. *Global and Planetary Change*, *101*, 72–81. https://doi.org/10.1016/j.gloplacha.2012.12.008

Huang, Y. F., Bond, D. P. G., Wang, Y. B., Wang, T., Yi, Z. X., Yuan, A. H., & Su, Y. Q. (2019). Early Triassic microbialites from the Changxing region of Zhejiang Province, South China. *Journal of Palaeogeography-English*, *8*, 22. https://doi.org/10.1186/s42501-019-0039-1

Jia, E. H., & Song, H. J. (2018). End-Permian mass extinction of calcareous algae and microproblematica from Liangfengya, South China. *Geobios*, *51*(5), 401–418. https://doi.org/10.1016/j.geobios.2018.08.007

Jiang, H. S., Lai, X. L., Sun, Y. D., Wignall, P. B., Liu, J. B., & Yan, C. B. (2014). Permian-Triassic conodonts from Dajiang (Guizhou, South China) and their implication for the age of microbialite deposition in the aftermath of the end-Permian mass extinction. *Journal of Earth Science*, *25*(3), 413–430. https://doi.org/10.1007/s12583-014-0444-4

Jiang, H. S., Lai, X. L., Yan, C. B., Aldridge, R. J., Wignall, P., & Sun, Y. D. (2011). Revised conodont zonation and conodont evolution across the Permian-Triassic boundary at the Shangsi section, Guangyuan, Sichuan, South China. *Global and Planetary Change*, *77*(3–4), 103–115. https://doi.org/10.1016/j.gloplacha.2011.04.003

Joachimski, M. M., Lai, X. L., Shen, S. Z., Jiang, H. S., Luo, G. M., Chen, B., et al. (2012). Climate warming in the latest Permian and the Permian-Triassic mass extinction. *Geology*, *40*(3), 195–198. https://doi.org/10.1130/g32707.1

Kaiho, K., Kajiwara, Y., Chen, Z. Q., & Gorjan, P. (2006). A sulfur isotope event at the end of the Permian. *Chemical Geology*, *235*, 33–47. https://doi.org/10.1016/j.chemgeo.2006.06.001

Kaiho, K., Oba, M., Fukuda, Y., Ito, K., Ariyoshi, S., Gorjan, P., et al. (2012). Changes in depth-transect redox conditions spanning the end-Permian mass extinction and their impact on the marine extinction: Evidence from biomarkers and sulfur isotopes. *Global and Planetary Change*, *94*(95), 20–32. https://doi.org/10.1016/j.gloplacha.2012.05.024

Lai, X. L., Yang, F. Q., Hallam, A., & Wignall, P. B. (1996). The Shangsi section, candidate of the global stratotype section and point of the Permian–Triassic boundary. In H. F. Yin (Ed.), *The Palaeozoic–Mesozoic Boundary, candidates of the global stratotype section and point of the Permian–Triassic boundary* (pp. 113–124). China University of Geosciences Press.

Lehrmann, D. J., Payne, J. L., Felix, S., Dillett, P. M., Wang, H., Yu, Y., & Wei, J. (2003). Permian–Triassic boundary sections from shallow-marine carbonate platforms of the Nanpanjiang basin, South China: Implications for oceanic conditions associated with the end-Permian extinction and its aftermath. *Palaeogeography, Palaeoclimatology, Palaeoecology*, *18*, 138–152.

Lehrmann, D. J., Wei, J., & Enos, P. (1998). Controls on facies architecture of a large Triassic carbonate platform; the Great Bank of Guizhou, Banpanjiang basin, South China. *Journal of Sedimentary Research*, *68*, 311–326.

Liao, W., Wang, Y. B., Kershaw, S., Weng, Z. T., & Yang, H. (2010). Shallow-marine dysoxia across the Permian-Triassic boundary: Evidence from pyrite framboids in the microbialite in South China. *Sedimentary Geology*, *232*(1–2), 77–83. https://doi.org/10.1016/j.sedgeo.2010.09.019

Liu, J. B., Ezaki, Y., Yang, S. R., Wang, H. F., & Adachi, N. (2007). Age and sedimentology of microbialites after the end-Permian mass extinction in Luodian, Guizhou Province. *Journal of Palaeogeography*, *9*, 473–486.

Liu, X. K., Song, H. J., Bond, D. P. G., Tong, J. N., & Benton, M. J. (2020). Migration controls extinction and survival patterns of foraminifers during the Permian-Triassic crisis in South China. *Earth-Science Reviews*, *209*, 103329. https://doi.org/10.1016/j.earscirev.2020.103329

Luo, H., Zhou, Z. C., Cai, H. W., Zhu, Y. H., Wang, Z. H., Chen, J. H., et al. (2013). Permian-Triassic boundary biostrarigraphy and sedimentology at the Yudongzi section of Jiangyou, Sichuan Province. *Journal of Stratigraphy*, *37*, 81–92.

Ma, D. R. (2016). *Uppermost Permian to lower Triassic conodonts from the Tieshikou section, southern Jiangxi Province and Selong section, southern Tibet*. China China University of Geosciences.

Ma, Y. S., Guo, X. S., Guo, T. L., Huang, R., Cai, X. Y., & Li, G. X. (2007). The Puguang gas field: New giant discovery in the mature Sichuan Basin, southwest China. *AAPG Bulletin*, *91*, 627–643.

Newton, R. J., Bond, D., Cope, H., & Wignall, P. B. (2009). A 'framboid gap' at the Permo-Triassic boundary. *Geochimica et Cosmochimica Acta*, *73*(13), 939.

Nicoll, R. S., Metcafle, I., & Wang, C. Y. (2002). New species of the conodont genus *Hindeodus* and conodont biostratigraphy of the Permian–Triassic boundary interval. *Journal of Asian Earth Sciences*, *20*, 609–631.

Payne, J. L., & Kump, L. R. (2007). Evidence for recurrent Early Triassic massive volcanism from quantitative interpretation of carbon isotope fluctuations. *Earth and Planetary Science Letters*, *256*(1–2), 264–277. https://doi.org/10.1016/j.epsl.2007.01.034

Payne, J. L., Lehrmann, D. J., Follett, D., Seibel, M., Kump, L. R., Riccardi, A., et al. (2007). Erosional truncation of uppermost Permian shallow-marine carbonates and implications for Permian–Triassic boundary events. *Geological Society of America Bulletin*, *119*, 771–784.

Pei, Y., Chen, Z. Q., Fang, Y. H., Kershaw, S., Wu, S. Q., & Luo, M. (2019). Volcanism, redox conditions, and microbialite growth linked with the end-Permian mass extinction: Evidence from the Xiajiacao section (western Hubei Province), South China. *Palaeogeography, Palaeoclimatology, Palaeoecology*, *519*, 194–208. https://doi.org/10.1016/j.palaeo.2017.07.020

Rong, H., Jiao, Y. Q., & Wu, L. Q. (2012). Effects of diagenesis on the acoustic velocity of the Triassic oolitic shoals in the Yudongzi outcrop of Erlangmiao area, northwest Sichuan Basin. *Journal of Earth Science*, *23*, 542–558.

Shen, J., Feng, Q. L., Algeo, T. J., Li, C., Planaysky, N. J., Zhou, L., & Zhang, M. L. (2016). Two pulses of oceanic environmental disturbance during the Permian-Triassic boundary crisis. *Earth and Planetary Science Letters*, *443*, 139–152. https://doi.org/10.1016/j.epsl.2016.03.030

Shen, W. J., Lin, Y. T., Xu, L., Li, J. F., Wu, Y. S., & Sung, Y. G. (2007). Pyrite framboids in the Permian-Triassic boundary section at Meishan, China: Evidence for dysoxic deposition. *Palaeogeography, Palaeoclimatology, Palaeoecology*, *253*(3–4), 323–331. https://doi.org/10.1016/j.palaeo.2007.06.005

Sheng, J., Chen, C., Wang, Y., Rui, L., Liao, Z., Bando, Y., et al. (1984). Permian–Triassic boundary in middle and eastern Tethys. *Journal of the Faculty of Science*, (Vol. *21*, pp. 133–181).

Song, H. J., Tong, J. N., Chen, Z. Q., Yang, H., & Wang, Y. B. (2009). End-Permian mass extinction of foraminifers in the Nanpanjiang basin, South China. *Journal of Paleontology*, *83*, 718–738.

Sun, C. L. (1988). Early Triassic stratigraphy in Jiangxi Province. *Journal of Stratigraphy*, *12*, 39–47.

Tang, H., Kershaw, S., Liu, H., Tan, X. C., Li, F., Hu, G., et al. (2017). Permian-Triassic boundary microbialites (PTBMs) in southwest China: Implications for paleoenvironment reconstruction. *Facies*, *63*(1), 2. https://doi.org/10.1007/s10347-016-0482-8

Tang, X. Y., Huang, J. H., Wang, Y. Z., Lu, Y. J., & Jin, F. (2007). Characteristics of inorganic carbon-isotope of the Permian- Triassic boundary in the Liangfengya section, Chongqing. *Geological Science and Technology Information*, *26*, 42–46.

Tian, L., Tong, J. N., Algeo, T. J., Song, H. J., Song, H. Y., Chu, D. L., et al. (2014). Reconstruction of Early Triassic ocean redox conditions based on framboidal pyrite from the Nanpanjiang Basin, South China. *Palaeogeography, Palaeoclimatology, Palaeoecology*, *412*, 68–79. https://doi.org/10.1016/j.palaeo.2014.07.018

Tian, L., Tong, J. N., Sun, D. Y., Xiong, Y. L., Wang, C. G., Song, H. J., et al. (2014). The microfacies and sedimentary responses to the mass extinction during the Permian-Triassic transition at Yangou Section, Jiangxi Province, South China. *Science China Earth Sciences*, *57*, 2195–2207.

Tong, J. N., Zakharov, Y. D., Orchard, M. J., Yin, H. F., & Hansen, H. J. (2003). A candidate of the Induan-Olenekian boundary stratotype in the Tethyan region. *Science in China (Series D)*, *46*, 1182–1200.

Tong, J. N., & Zhao, L. S. (2011). Lower Triassic and Induan-Olenekian boundary in Chaohu, Anhui Province, South China. *Acta Geologica Sinica*, *85*, 801–840.

Tong, J. N., Zuo, J. X., & Chen, Z. Q. (2007). Early Triassic carbon isotope excursions from South China: Proxies for devastation and restoration of marine ecosystems following the end-Permian mass extinction. *Geological Journal*, *42*(3–4), 371–389. https://doi.org/10.1002/gj.1084

Wang, L. N., Wignall, P. B., Wang, Y. B., Jiang, H. S., Sun, Y. D., Li, G. S., et al. (2016). Depositional conditions and revised age of the Permo-Triassic microbialites at Gaohua section, Cili County (Hunan Province, South China). *Palaeogeography, Palaeoclimatology, Palaeoecology*, *443*, 156–166. https://doi.org/10.1016/j.palaeo.2015.11.032

Wang, X. D., Cawood, P. A., Zhao, H., Zhao, L. S., Grasby, S. E., Chen, Z. Q., & Zhang, L. (2019). Global mercury cycle during the end-Permian mass extinction and subsequent Early Triassic recovery. *Earth and Planetary Science Letters*, *513*, 144–155. https://doi.org/10.1016/j.epsl.2019.02.026

Wei, H. Y., Algeo, T. J., Yu, H., Wang, J. G., Guo, C., & Shi, G. (2015). Episodic euxinia in the Changhsingian (late Permian) of South China: Evidence from framboidal pyrite and geochemical data. *Sedimentary Geology*, *319*, 78–97. https://doi.org/10.1016/j.sedgeo.2014.11.008

Wignall, P. B., & Hallam, A. (1996). Facies change and the end-Permian mass extinction in SE Sichuan, China. *PALAIOS*, *11*(6), 587–596. https://doi.org/10.2307/3515193

Wignall, P. B., Kershaw, S., Collin, P. Y., & Crasquin-Soleau, S. (2009). Comment: Erosional truncation of uppermost Permian shallow-marine carbonates and implications for Permian–Triassic boundary events. *Geological Society of America Bulletin*, *121*, 954–956.

Wu, G. C., Yao, J. X., & Ji, Z. S. (2003). Conodont fauna of late upper Permian in Xinfeng area, Jiangxi Province. *Acta Scientiarum Naturalium Universitatis Pekinensis*, *39*, 211–218.

Wu, S. Q., Chen, Z. Q., Fang, Y. H., Pei, Y., Yang, H., & Ogg, J. (2017). A Permian-Triassic boundary microbialite deposit from the eastern Yangtze Platform (Jiangxi Province, South China): Geobiologic features, ecosystem composition and redox conditions. *Palaeogeography, Palaeoclimatology, Palaeoecology*, *486*, 58–73. https://doi.org/10.1016/j.palaeo.2017.05.015

Wu, Y. S., Jiang, H. X., Yang, W., & Fan, J. S. (2007). Microbialite of anoxic condition from Permian-Triassic transition in Guizhou, China. *Science in China - Series D: Earth Sciences*, *50*(7), 1040–1051. https://doi.org/10.1007/s11430-007-0033-9

Xiang, L., Schoepfer, S. D., Zhang, H., Yuan, D. X., Cao, C. Q., Zheng, Q. F., et al. (2016). Oceanic redox evolution across the end-Permian mass extinction at Shangsi, South China. *Palaeogeography, Palaeoclimatology, Palaeoecology*, *448*, 59–71. https://doi.org/10.1016/j.palaeo.2015.10.046

Xiao, Y. F., Wu, K., Tian, L., Benton, M. J., Du, Y., Yang, H., & Tong, J. N. (2018). Framboidal pyrite evidence for persistent low oxygen levels in shallow marine facies of the Nanpanjiang Basin during the Permian-Triassic transition. *Palaeogeography, Palaeoclimatology, Palaeoecology*, *511*, 243–255. https://doi.org/10.1016/j.palaeo.2018.08.012

Yin, H., Zhang, K., Tong, J., Yang, Z., & Wu, S. (2001). The global stratotype section and point (GSSP) of the Permian–Triassic boundary. *Episodes*, *24*, 102–114.

Yuan, D. X., & Shen, S. Z. (2011). Conodont succession across the Permian–Triassic boundary of the Liangfengya section, Chongqing, South China. *Acta Palaeontologica Sinica*, *50*, 420–438.

Zhao, L., Chen, Z. Q., Algeo, T. J., Chen, J., Chen, Y., Tong, J., et al. (2013). Rare-earth element patterns in conodont albid crowns: Evidence for massive inputs of volcanic ash during the latest Permian biocrisis? *Global and Planetary Change*, *105*, 135–151. https://doi.org/10.1016/j.gloplacha.2012.09.001

Zhou, W., Algro, T. J., Ruan, X., Luo, G., Chen, Z. Q., & Xie, S. C. (2017). Expansion of photic-zone euxinia during the Permian–Triassic biotic crisis and its causes: Microbial biomarker records. *Palaeogeography, Palaeoclimatology, Palaeoecology*, *474*, 140–151. https://doi.org/10.1016/j.palaeo.2016.06.027

Zhu, X. S., Zhang, D. F., & Zhong, Y. X. (1999). Discoveries of the *Clarkina* from the P/T boundary clay bed in Taojiang section in southern Jiangxi. *Journal of Jiangxi Normal University*, *23*, 162–169.